Modeling the conductivity around the dimensionality-controlled metal-insulator transition in $LaNiO_3/LaAlO_3$ (100) superlattices

Haoming Wei, Marcus Jenderka, Michael Bonholzer, Marius Grundmann, and Michael Lorenz

Citation: Appl. Phys. Lett. **106**, 042103 (2015); doi: 10.1063/1.4907011

View online: https://doi.org/10.1063/1.4907011

View Table of Contents: http://aip.scitation.org/toc/apl/106/4

Published by the American Institute of Physics

Modeling the conductivity around the dimensionality-controlled metal-insulator transition in $LaNiO_3/LaAlO_3$ (100) superlattices

Haoming Wei, Marcus Jenderka, Michael Bonholzer, Marius Grundmann, and Michael Lorenz[a)]
Semiconductor Physics Group, Institut für Experimentelle Physik II, Universität Leipzig, Linnéstr. 5, D-04103 Leipzig, Germany

(Received 12 December 2014; accepted 19 January 2015; published online 28 January 2015)

A dimensionality controlled metal insulator transition in epitaxial $[LaNiO_3$ (d nm)/$LaAlO_3$(2 nm)$]_{10}$ (100) superlattices (thereafter $[d/2]_{10}$ SLs) is demonstrated for decreasing $LaNiO_3$ single layer thickness from 4 nm down to 1.2 nm. The $[4/2]_{10}$ SL shows metallic behavior with positive resistivity temperature coefficient, while the $[2/2]_{10}$ SL shows a metal-insulator transition with crossover from 3D to two-dimensional single-layer dimensionality. Strong localization appears for the $[1.2/2]_{10}$ SL with the resistivity being dominated by two-dimensional variable range hopping with a localization length of about 0.035 nm. © *2015 AIP Publishing LLC*. [http://dx.doi.org/10.1063/1.4907011]

$LaNiO_3$ (LNO) is an interesting material exhibiting Pauli paramagnetic metallic behavior in a wide temperature range.[1] Consequently, research interest in LNO is focussed, for example, on highly conductive electrodes for ferroelectric thin-film devices.[2] Recently, LNO-based superlattices (SLs) have drawn enormous attention since the possibility of high-temperature superconductivity was predicted.[3,4] Furthermore, electronic structure calculations propose the appearance of correlation-driven topological phases in $LaNiO_3/LaAlO_3$ (LAO) bilayer structures, where LAO is a wide band-gap insulator.[5,6] Most recently, density functional theory calculations predict a set of broken-symmetry two-dimensional ground states in LNO_N/LAO_M (111) superlattices.[7] In dependence on number of LNO layers in the SL being 1, 2, and ≥ 3, ferromagnetic Mott insulating, switchable multiferroic, and a metal-insulator transition (MIT) through a half-semimetallic phase are proposed.[7]

Little experimental work has been performed up to now to verify these theoretical predictions. In 2008, Tsubouchi *et al*. reported epitaxial growth control of LNO films using pulsed laser deposition (PLD) with *in situ* high-pressure reflection high-energy electron diffraction (RHEED).[8] Layer-by-layer growth was identified by intensity oscillations of the RHEED specular spot during deposition. The LNO films are metallic with uniform Ni^{3+} oxidation state and maintain an atomically flat surface. Scherwitzl *et al*. grew ultrathin LNO films by off-axis rf magnetron sputtering and investigated transport behavior of these single LNO films.[9] Son *et al*. fabricated [LNO(4 u.c.)/$SrTiO_3$ (STO) (3 u.c.)] SLs in 2010.[10] The conductivity of SLs was enhanced compared to single LNO layers of the same thickness due to electron tunneling through the STO barrier. Liu *et al*. reported epitaxial growth of [LNO(1 u.c.)/LAO(1 u.c.)] SLs on polar LAO and non-polar STO substrate by interval PLD.[11] The influence of polar mismatch on the electronic and structural properties of SLs was studied in detail. More recently, *ab initio* cluster calculations together with absorption spectra were used to study the quantum confinement of Mott electrons in $[(LNO)_n/(LAO)_3]$ SLs.[12] Furthermore, electronic phase transitions in nickel-oxide superlattices were studied by optical ellipsometry and low-energy muon spin rotation.[13] Collective metal-insulator and antiferromagnetic transitions were observed as a function of temperature in systems with lowered dimensionality.[13] In their experiment, $SrTiO_3$ and $LaSrAlO_4$ single crystals are used as the substrate.[13] However, the effect of the substrate on the electrical sample properties is not clear. Oxygen vacancies in $SrTiO_3$ may result in a conducting interface, and degradation or dissolution of $LaSrAlO_4$ cannot be excluded because it is a deliquescent material.

In this letter, we report on the epitaxial growth of $[LaNiO_3$ (d nm)/$LaAlO_3$ (2 nm)$]_{10}$ (100) SLs and the corresponding single layers. The SLs are in the following referred to as $[d/2]_{10}$. By lowering the dimensionality of the LNO layers in the SLs from 3D to two-dimensional (2D), a metal-insulator transition depending on the confinement is observed. The intrinsic conductivity mechanisms around the transition are discussed by means of appropriate modeling for the different dimensionalities.

Sample growth was done by PLD using a KrF excimer laser operating at 248 nm wavelength and 600 mJ pulse energy, see Ref. 14 and articles therein. Stoichiometric LAO and LNO targets were prepared by the solid-state reaction of high-purity (4N) La_2O_3, Al_2O_3, and NiO powders. LAO, $(LaAlO_3)_{0.3}(Sr_2AlTaO_6)_{0.7}$ (LSAT), and STO single crystals with (100) orientation were used as substrates. Before deposition, substrates were annealed in order to obtain a terraced surface with monolayer steps. *In-situ* high-pressure RHEED (STAIB Torr RHEED) was used to monitor the growth process. Depositions were done at temperatures of about 680 °C and oxygen pressures of 3×10^{-4} mbar for LAO and 0.05 mbar for LNO. After deposition, samples were annealed in 800 mbar oxygen atmosphere at 680 °C for 15 min to improve the quality of films and to reduce the inherent oxygen deficit of PLD-grown transition-metal oxide films.[15]

[a)]Author to whom correspondence should be addressed. Electronic mail: mlorenz@physik.uni-leipzig.de.

The structure and orientation of the samples were examined by wide-angle XRD using a Philips X'Pert diffractometer with Cu-Kα radiation and a Bragg-Brentano goniometer with focusing beam optics and secondary graphite monochromator. Reciprocal space maps (RSMs) were recorded with a PANalytical X'pert PRO Materials Research Diffractometer using Cu-Kα radiation from a parabolic mirror and a PIXcel^{3D} multichannel detector. The surface morphology and layer thickness were investigated by AFM in dynamic non-contact mode (Park System XE-150) and X-ray reflectivity (XRR), respectively. Temperature dependent DC electrical resistivity was measured in Van der Pauw geometry using a Hall setup. For these electrical measurements, samples on LAO were used in contrast to the previous work[9,13] to ensure in-plane lattice match to the LAO layers and to induce compressive strain in the LNO layers.

Fig. 1(a) shows the intensity of the RHEED specular (0,0) spot during LAO growth at an oxygen pressure of 3×10^{-4} mbar. The 2D layer-by-layer growth is indicated by the oscillations for the first few LAO monolayers. The damping of the oscillations denotes the beginning of formation of multi-level steps. The sharp RHEED patterns with clear Kikuchi lines in inset of Fig. 1(a) confirm an atomically flat film surface, see Fig. 1(c). The thickness of LAO and LNO thin films is estimated from the numbers of applied laser pulses and double checked by XRR measurement. Fig. 1(b) shows XRD 2θ-ω-scans through the (200) symmetric reflections of LAO substrate and LAO films with variable thickness, but otherwise identical PLD parameters. All LAO films have consistent out-of-plane lattice constant which is independent of thickness. As shown in the AFM images in Fig. 1(c), the LAO films have smooth surface with root mean square (rms) roughness below 0.17 nm up to 600 nm thickness. Streaky RHEED patterns were observed during LNO growth as shown in Fig. 1(d). The epitaxial LNO films show (100) out-of-plane crystalline orientation

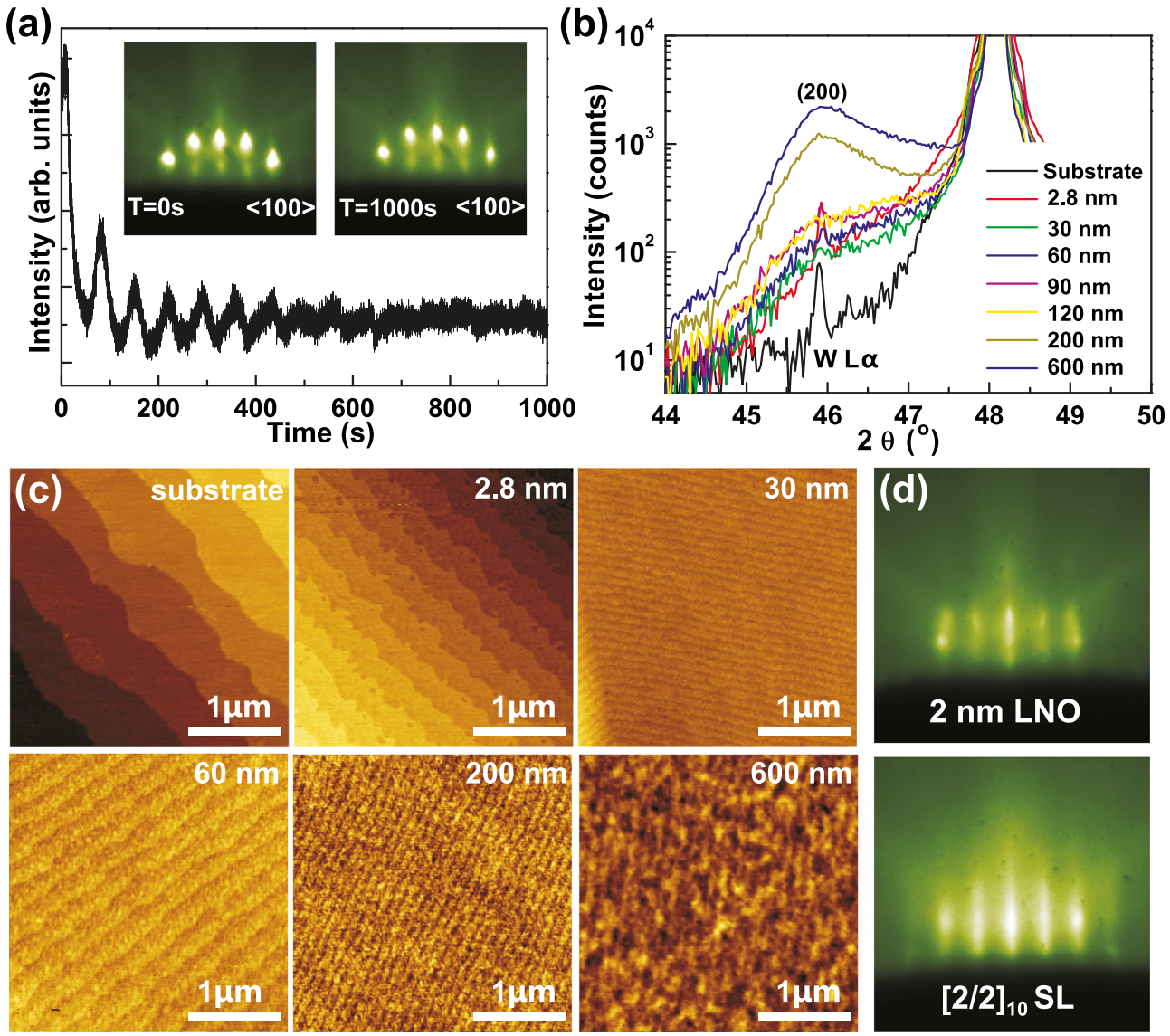

FIG. 1. (a) RHEED oscillations of 14 monolayers LAO of 0.395 nm grown homoepitaxially on LAO substrate. The insets are *in-situ* RHEED patterns before and after deposition. (b) XRD 2θ-ω-scans of annealed LAO substrate and thin films with thickness from 2.8 to 600 nm. (c) AFM images of LAO substrate and thin films with indicated thickness. The step height corresponds for all images to one LAO monolayer. (d) RHEED patterns of 2 nm thin LNO film and $[2/2]_{10}$ SL deposited on STO (100) substrate.

and in-plane epitaxial relationship similar to those of our previous work.[16] Combining the optimized LNO and LAO growth, $[LNO/LAO]_{10}$ (100) SLs were fabricated.

Fig. 2(a) displays the XRD 2θ-ω-scans of the $[2/2]_{10}$ SL on LSAT substrate. The main peak of the SL appears close to the LSAT substrate peak indicated by the black XRD pattern. Moreover, satellite peaks up to third order are observed which indicate smooth interfaces between the LAO and the LNO layers. From the distance between adjacent satellite peaks, the thickness of one LNO/LAO double layer is estimated to be 4.00 ± 0.03 nm, which is fully consistent with our design of 2 nm LAO and 2 nm LNO. In addition, XRR was used to determine more precisely the SL structure, thickness, and interfacial roughness as shown in the inset of Fig. 2(a). Strong Bragg reflections, arising from the difference in mass densities of LNO and LAO, are obtained indicating abrupt interfaces. The single layer thickness of LAO and LNO is 2 ± 0.01 nm and 2 ± 0.02 nm, and interfacial roughness is in between 0.37 and 0.54 nm, i.e., in the range of one monolayer within the large XRR focus of $5 \times 2\,mm^2$. For comparison, an interface roughness around 1 unit cell was also estimated in supplementary material of Ref. 13 from their XRR analysis. Interface quality of all samples used here in this work is expected to be very similar, as we conclude from surface roughness measured by AFM.

Fig. 2(b) shows a typical RSM collected around the asymmetric (−103) LSAT substrate peak. The RSM clearly reveals that the in-plane lattice parameter of the SL is identical to that of the substrate, indicating that the SL is coherently grown on the single-crystalline LSAT substrate. For LAO substrate, we could confirm pseudomorphic, i.e., lattice matched growth as well.

Fig. 3 displays in-plane resistivity (ρ) of LNO single films and SLs deposited on LAO substrates as a function of temperature for decreasing LNO layer thickness down to 1.2 nm, i.e., three monolayers. All LNO single films show metallic conductivity in the measured temperature range from less than 50 K to 300 K. For modeling of conductivity of thick LNO films, see the former papers.[16,17] In the following, we discuss the extension of Ref. 16 to lower LNO thickness. At temperatures above 100 K, ρ(T) follows the linear relation: $\rho = \rho_0 + AT$. Such a behavior of ρ is related to electron-phonon (*el-ph*) scattering. The *el-ph* coupling λ can be estimated from the slope of the resistivity using:[18] $\lambda = (\hbar\omega_P{}^2/8\pi^2 k_B)[\rho(T) - \rho(0)]/T = 0.246(\hbar\omega_P)^2 A$, where $\hbar\omega_P$ is the plasmon energy, ω_P is the plasmon frequency, k_B is the Boltzmann constant, and A is the slope of ρ(T). The mean free path l can be obtained by using the relation:[18] $l = 4.95 \times 10^{-4}\, \upsilon_F/\rho\ (\hbar\omega_P)^2$, where υ_F is the Fermi velocity (about 1.05×10^{-7} cm s^{-1} for LNO). The mean free path decreases with decreasing thickness as can be seen in Table I. The deviation from linear relation at low temperatures (below 67 K) is due to the electron-electron (*el-el*) Coulomb interaction that is related to 3*d* electrons.[19]

Interestingly, the dependence of resistivity of the SLs with temperature is drastically changed. With decreasing thickness of LNO layers in the SLs, a metal-insulator transition occurs at $d = 2$ nm. The difference in resistivity can be as large as seven orders of magnitude. This feature emphasizes the significance of size effects on the electric transport of oxide SLs and indicates changing conductivity

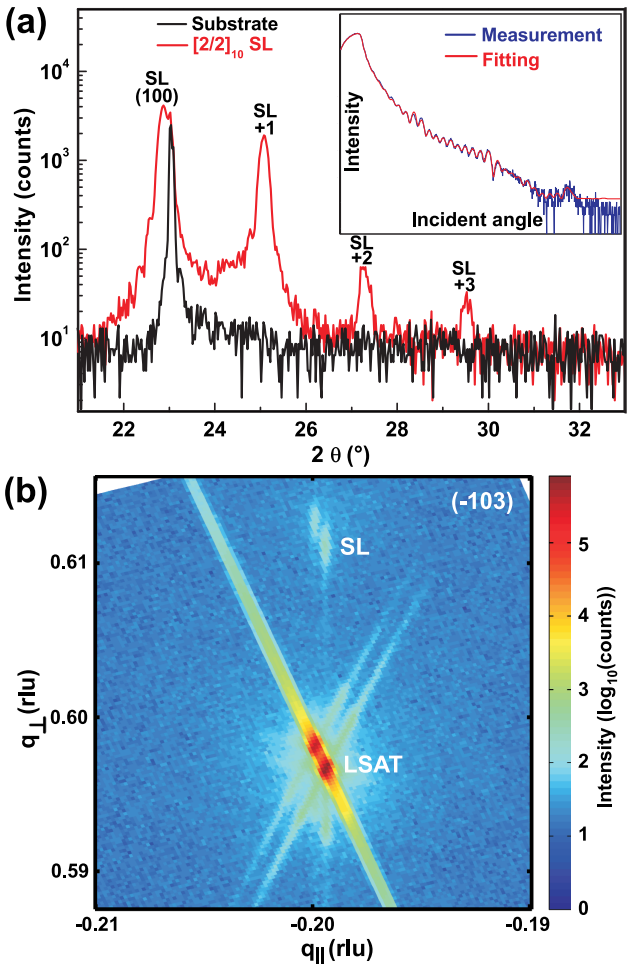

FIG. 2. (a) XRD 2θ-ω-scans of $[2/2]_{10}$ SL on LSAT (100) substrate. The inset shows the corresponding X-ray reflectivity measurement and model fit. (b) RSM of $[2/2]_{10}$ SL around the asymmetric LSAT (−103) peak. The double-peak structure of both substrate and SL peaks refers to $K\alpha_{1/2}$ splitting of incident X-ray parallel beam.

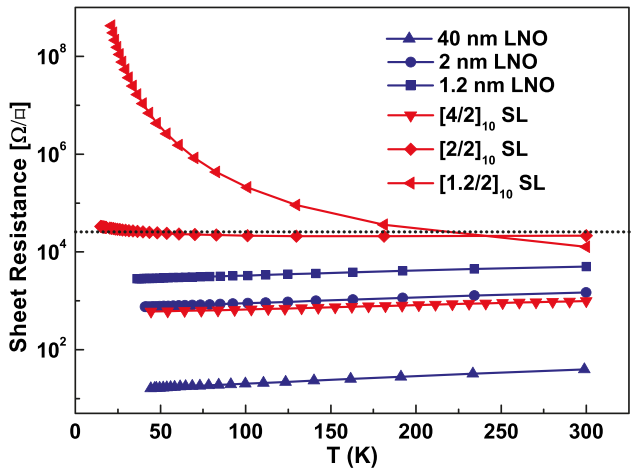

FIG. 3. Temperature-dependent resistivity of single LNO films and LNO/LAO SLs with indicated thickness down to 3 unit cells. All samples are deposited on LAO which induces in-plane compressive strain in LNO films and SLs. The horizontal black dotted line corresponds to 25.8 kΩ/□, the quantum of resistance in 2D state.

TABLE I. Electrical characteristics of the single LNO films with decreasing thickness: resistivity ρ, *el-ph* coupling constant λ, and carriers mean free path l (at 300 K).

Thickness (nm)	ρ (T = 300 K) ($\mu\Omega$ cm)	λ ($\times 10^{-3}$)	l (T = 300 K) (Å)
40	159	97 ± 2.5	32.7 ± 0.1
2	298	148 ± 2.5	17.4 ± 0.3
1.2	602	255 ± 2.3	8.6 ± 0.1

mechanisms, which will be discussed in the following. Assuming that the weak scattering theory for conductivity (according to Boltzmann transport) is still adequate, the conductivity of a 2D electron gas is given by:[20] $\sigma = e^2 k_F l/h$, where k_F is the wave number of electrons on the Fermi surface and l is the mean free path. Ioffe and Regel point out that $k_F l$ cannot be significantly less than unity.[21] If $k_F l$ is close to unity, a MIT is expected. In this case, the maximum sheet resistance of a metallic conductor approaches $h/e^2 \approx 25.8\,\text{k}\Omega/\square$, which is the quantum of resistance in 2D state.[9] As can be seen in Fig. 3, the sheet resistivity of $[4/2]_{10}$ SL is much lower than the critical value (h/e^2), and metallic behavior is found at all temperatures. When the sheet resistivity is close to h/e^2, the $[2/2]_{10}$ SL undergoes a transformation from metallic to insulating state. In contrast, the $[1.2/2]_{10}$ SL which is considered to be insulating shows a strong increase in resistance with decreasing temperature.

In order to clarify the intrinsic conductivity mechanism of the SLs for different LNO thicknesses, the temperature-dependent resistivity is fitted by appropriate models as shown in Fig. 4. We like to mention again that for thick metallic LNO films, the resistivity is proportional to the square of temperature at low temperatures.[16,19] However, the resistivity of $[4/2]_{10}$ SL is well described by $\rho = \rho_0 + BT^{3/2}$ as shown in Fig. 4(a), which is attributed to scattering of the Fermi liquid electrons to form bond-length fluctuations.[22] This phenomenon is associated with strong-correlation fluctuations and indicates enhanced electronic correlations in the quantum confinement regime.[10,22] Similar behavior has been observed in [LNO/$SrMnO_3$] SLs.[23]

The $[2/2]_{10}$ SL shows insulating behavior at low temperatures with the transition temperature from metallic to insulating at about 180 K as shown in Fig. 3. This MIT phenomenon is related to the weak localization effect where quantum interference of electronic waves diffusing around impurities enhances backscattering and leads to a reduction of the conductivity.[24] As shown in Fig. 4(b), the 2D zero-field conductivity shows a logarithmic increase as temperature increases:[25] $\sigma = \sigma_0 + p\frac{e^2}{\pi h}\ln\left(\frac{T}{T_0}\right)$, where σ_0 is the Drude conductivity and p is an index depending on scattering mechanism. If the main inelastic relaxation mechanism is due to *el-el* collisions, $p = 1$, whereas *el-ph* scattering gives $p = 3$. Fig. 4(b) shows the sheet conductance as a function of $\ln(T)$. Linear fitting of our data yields a slope of 9.8 ± 0.1 μS. The calculated value of p is 0.9 ± 0.01, which is close to 1. According to this, the conductivity at low temperatures is dominated by *el-el* collisions.

Fig. 4(c) shows the sheet conductance of the $[1.2/2]_{10}$ SL as a function of temperature. Variable range hopping (VRH) transport has been observed in both ultrathin LNO films and [LNO/$SrMnO_3$] SLs.[9,23] At low temperatures, electrons hop between localized states and the sheet conductance is given by:[26] $\sigma = \sigma_0 \exp[-(T_0/T)^{\alpha}]$. For d-dimensional systems, the exponent $\alpha = 1/(d+1)$. The 2D VRH equation fits the low T data from 23 to 130 K well as can be seen in Fig. 4(c). The slope and T_0 value obtained by fitting the resistivity curve are 50.1 ± 0.2 and (1.26 ± 0.01) × 10^5 K. Large deviations exist if we fit the data with a 3D expression, indicating that coupling of the LNO layers through the 2 nm thick LAO layers is largely suppressed. For the 2D VRH model, T_0 is given by:[27] $T_0 = 13.8/k_B N(E_F)\, a^2$, where $N(E_F)$ is the density of localized states at the Fermi level and a is the localization length. As a rough approximation, $N(E_F)$ is about $1.02 \times 10^{21}\,\text{eV}^{-1}$ that was calculated using:[28] $k_B N(E_F) = \partial n/\partial T \approx n(100\,\text{K})/100\,\text{K}$. Thus, the calculated localization length a of our $[2/2]_{10}$ SL is about 0.35 Å. According to the

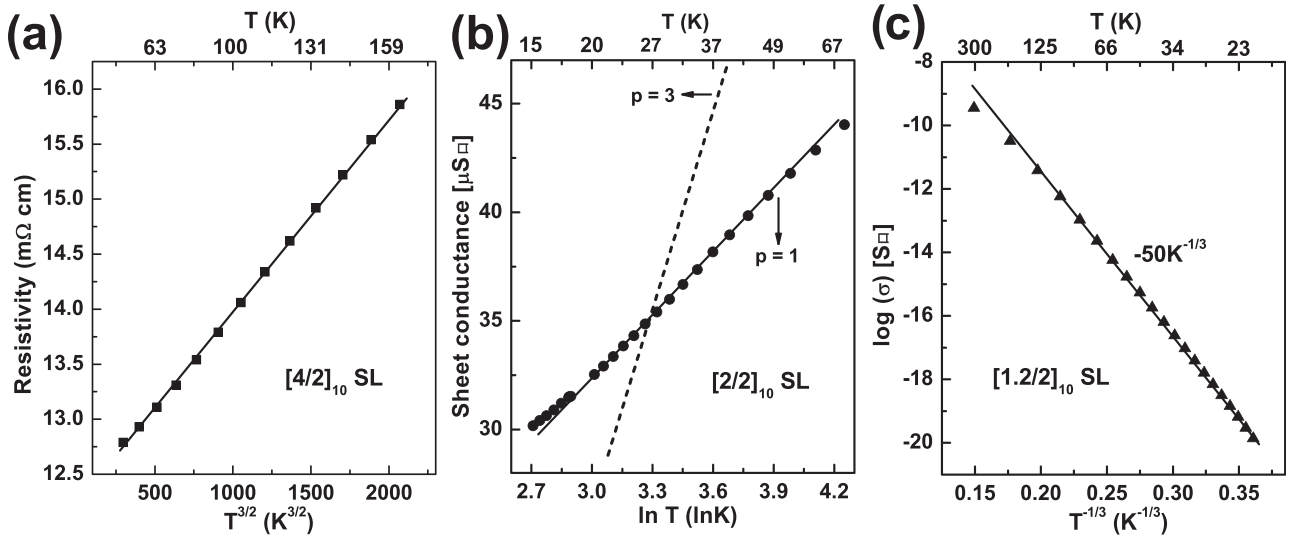

FIG. 4. Modeling of SL conductivity for decreasing LNO layer thickness from 4 down to 1.2 nm, for the indicated temperature ranges: (a) Temperature-dependent resistivity $\rho \propto T^{3/2}$ of $[4/2]_{10}$ SL. (b) Sheet conductance versus the logarithm of temperature $\ln(T)$ for $[2/2]_{10}$ SL. (c) Logarithm of conductance $\log(\sigma)$ as a function of $1/T^{1/3}$ of $[1.2/2]_{10}$ SL.

VRH theory, the mean hopping distance R_{hop} must be larger than the localization length a, which is given by: $R_{hop} = \frac{1}{3}a\left(\frac{T_0}{T}\right)^{1/3}$.[29] The ratio of R_{hop}/a is larger than 2.49 within the temperature range, which satisfies the requirement of VRH theory. Furthermore, the hopping energy for 2D VRH is given by: $E_{hop} = \frac{1}{3}k_B T^{2/3} T_0^{1/3}$.[30] The ratio of E_{hop}/k_B is also larger than 1 even at 300 K, which verifies once more the validity of the 2D VRH mechanism. It is worth to mention that metal-insulator transitions were also observed for the SLs deposited on LSAT substrates which induce tensile strain. However, transition temperature is about 230 K which is higher than that of SLs deposited on LAO substrate. This difference may be related to the different substrate-induced strain of the films.

In summary, we have demonstrated epitaxial and lattice matched growth of single LAO and $LaNiO_3$ films and superlattices with controlled single layer thickness down to three monolayers. Sharp RHEED patterns and AFM images confirm an atomically flat surface. XRD reciprocal space maps reveal the in-plane lattice match of the superlattices to the substrates. X-ray reflectivity data with strong Bragg reflections indicate abrupt interfaces of SLs with interfacial roughness in the order of one unit cell. A clear quantum confinement effect on the electronic properties including a metal-insulator transition of the LNO/LAO SLs is demonstrated for decreasing LNO thickness. Single LNO films and SLs with LNO thickness of 4 nm show metallic behavior at all temperatures. The SL with 2 nm thick LNO shows a metal-insulator transition due to the quantum interference of electronic waves. Strong localization appears when the LNO thickness of superlattices is reduced to 1.2 nm, i.e., to 3 unit cells, and 2D variable range hopping is the dominant conduction mechanism. The experimental findings and the modeling clearly demonstrate that dimensionality at the atomic scale is a key parameter to control the electronic structure in oxide superlattices, thus opening possibilities for design and control of transport properties in these systems, and to deepen their basic understanding.

We thank the Deutsche Forschungsgemeinschaft (DFG) for financial support within the Collaborative Research Center SFB 762 "Functionality of Oxide Interfaces" and the project LO790/5-1 "Oxide topological insulator thin films."

[1]D. G. Ouellette, S. B. Lee, J. Son, S. Stemmer, L. Balents, A. J. Millis, and S. J. Allen, Phys. Rev. B **82**, 165112 (2010).
[2]Y. W. Li, Z. G. Hu, J. L. Sun, X. J. Meng, and J. H. Chu, Appl. Phys. Lett. **92**, 042901 (2008).
[3]M. Gibert, P. Zubko, R. Scherwitzl, J. Iniguez, and J. M. Triscone, Nat. Mater. **11**, 195 (2012).
[4]E. Sakai, M. Tamamitsu, K. Yoshimatsu, S. Okamoto, K. Horiba, M. Oshima, and H. Kumigashira, Phys. Rev. B **87**, 075132 (2013).
[5]K. Y. Yang, W. Zhu, D. Xiao, S. Okamoto, Z. Wang, and Y. Ran, Phys. Rev. B **84**, 201104(R) (2011).
[6]A. Ruegg, C. Mitra, A. A. Demkov, and G. A. Fiete, Phys. Rev. B **85**, 245131 (2012).
[7]D. Doenning, W. E. Pickett, and R. Pentcheva, Phys. Rev. B **89**, 121110(R) (2014).
[8]K. Tsubouchi, I. Ohkubo, H. Kumigashira, Y. Matsumoto, T. Ohnishi, M. Lippmaa, H. Koinuma, and M. Oshima, Appl. Phys. Lett. **92**, 262109 (2008).
[9]R. Scherwitzl, S. Gariglio, M. Gabay, P. Zubko, M. Gibert, and J. M. Triscone, Phys. Rev. Lett. **106**, 246403 (2011).
[10]J. Son, J. M. LeBeau, S. J. Allen, and S. Stemmer, Appl. Phys. Lett. **97**, 202109 (2010).
[11]J. Liu, M. Kareev, S. Prosandeev, B. Gray, P. Ryan, J. W. Freeland, and J. Chakhalian, Appl. Phys. Lett. **96**, 133111 (2010).
[12]J. Liu, S. Okamoto, M. V. Veenendaal, M. Karrev, B. Gray, P. Ryan, J. W. Freeland, and J. Chakhalian, Phys. Rev. B **83**, 161102(R) (2011).
[13]A. V. Boris, Y. Matiks, E. Benckiser, A. Frano, P. Popovich, V. Hinkov, P. Wochner, M. C. Colin, E. Detemple, V. K. Malik, C. Bernhard, T. Prokscha, A. Suter, Z. Salman, E. Morenzoni, G. Cristiani, H. U. Habermeier, and B. Keimer, Science **332**, 937–940 (2011).
[14]M. Lorenz and R. Rao, J. Phys. D: Appl. Phys. **47**, 030301 (2014).
[15]M. Lorenz, R. Böttcher, S. Friedländer, A. Pöppl, D. Spemann, and M. Grundmann, J. Mater. Chem. C **2**, 4947 (2014).
[16]H. M. Wei, M. Jenderka, M. Grundmann, and M. Lorenz, "$LaNiO_3$ films with tunable out-of-plane lattice parameter and their strain- related electrical properties," Phys. Status Solidi A (submitted).
[17]G. P. Mambrini and E. R. Leite, J. Appl. Phys. **102**, 043708 (2007).
[18]M. Gurvitch and A. T. Fiory, Phys. Rev. Lett. **59**, 1337 (1987).
[19]L. Qiao and X. Bi, Europhys. Lett. **93**, 57002 (2011).
[20]D. C. Licciardello and D. J. Thouless, Phys. Rev. Lett. **35**, 1475 (1975).
[21]A. A. Gogolin, Z. Phys. B - Condensed Matter **52**, 19–29 (1983).
[22]F. Rivadulla, J. S. Zhou, and J. B. Goodenough, Phys. Rev. B **67**, 165110 (2003).
[23]S. J. May, T. S. Santos, and A. Bhattacharya, Phys. Rev. B **79**, 115127 (2009).
[24]R. Scherwitzl, P. Zubko, C. Lichtensteiger, and J. M. Triscone, Appl. Phys. Lett. **95**, 222114 (2009).
[25]P. A. Lee, Rev. Mod. Phys. **57**, 287 (1985).
[26]W. Brening, Philos. Mag. **27**, 1093 (1973).
[27]M. I. B. Utama, X. Lu, D. Zhan, S. T. Ha, Y. Yuan, Z. Shen, and Q. Xiong, Nanoscale **6**, 12376–12382 (2014).
[28]G. Eda, C. Mattevi, H. Yamaguchi, H. Kim, and M. Chhowalla, J. Phys. Chem. C **113**, 15768 (2009).
[29]Z. H. Khan, M. Husain, T. P. Perng, N. Salah, and S. Habib, J. Phys.: Condens. Matter **20**, 475207 (2008).
[30]S. J. Lee and J. B. Ketterson, Phys. Rev. B **46**, 12695 (1992).